



HAL
open science

LPMO-oxidized cellulose oligosaccharides evoke immunity in Arabidopsis conferring resistance towards necrotrophic fungus *B. cinerea*

Marco Zarattini, Massimiliano Corso, Marco Antonio Kadowaki, Antonielle Monclaro, Silvia Magri, Irma Milanese, Sylvie Jolivet, Mariana Ortiz de Godoy, Christian Hermans, Mathilde Fagard, et al.

► To cite this version:

Marco Zarattini, Massimiliano Corso, Marco Antonio Kadowaki, Antonielle Monclaro, Silvia Magri, et al.. LPMO-oxidized cellulose oligosaccharides evoke immunity in Arabidopsis conferring resistance towards necrotrophic fungus *B. cinerea*. *Communications Biology*, 2021, 4 (1), pp.727. 10.1038/s42003-021-02226-7. hal-03738681

HAL Id: hal-03738681

<https://hal.inrae.fr/hal-03738681>

Submitted on 9 Feb 2024





HAL is a multi-disciplinary open access archive for the deposit and dissemination of scientific research documents, whether they are published or not. The documents may come from teaching and research institutions in France or abroad, or from public or private research centers.

L'archive ouverte pluridisciplinaire **HAL**, est destinée au dépôt et à la diffusion de documents scientifiques de niveau recherche, publiés ou non, émanant des établissements d'enseignement et de recherche français ou étrangers, des laboratoires publics ou privés.



Distributed under a Creative Commons Attribution 4.0 International License

LPMO-oxidized cellulose oligosaccharides evoke immunity in *Arabidopsis* conferring resistance towards necrotrophic fungus *B. cinerea*

Marco Zarattini¹ , Massimiliano Corso² , Marco Antonio Kadowaki¹, Antonielle Monclaro¹, Silvia Magri¹, Irma Milanese¹, Sylvie Jolivet², Mariana Ortiz de Godoy¹, Christian Hermans³, Mathilde Fagard² & David Cannella¹  

Lytic Polysaccharide Monooxygenases (LPMOs) are powerful redox enzymes able to oxidatively cleave recalcitrant polysaccharides. Widely conserved across biological kingdoms, LPMOs of the AA9 family are deployed by phytopathogens to deconstruct cellulose polymers. In response, plants have evolved sophisticated mechanisms to sense cell wall damage and thus self-triggering Damage Triggered Immunity responses. Here, we show that *Arabidopsis* plants exposed to LPMO products triggered the innate immunity ultimately leading to increased resistance to the necrotrophic fungus *Botrytis cinerea*. We demonstrated that plants undergo a deep transcriptional reprogramming upon elicitation with AA9 derived cellulose- or cello-oligosaccharides (AA9_COS). To decipher the specific effects of native and oxidized LPMO-generated AA9_COS, a pairwise comparison with cellobiose, the smallest non-oxidized unit constituting cellulose, is presented. Moreover, we identified two leucine-rich repeat receptor-like kinases, namely STRESS INDUCED FACTOR 2 and 4, playing a crucial role in signaling the AA9_COS-dependent responses such as camalexin production. Furthermore, increased levels of ethylene, jasmonic and salicylic acid hormones, along with deposition of callose in the cell wall was observed. Collectively, our data reveal that LPMOs might play a crucial role in plant-pathogen interactions.

¹ PhotoBioCatalysis Unit—BioCat, Crop Production and Biostimulation Laboratory CPBL and BTL, Université libre de Bruxelles, Brussels, Belgium. ² Institut Jean-Pierre Bourgin, Université Paris-Saclay, INRAE, AgroParisTech, Versailles, France. ³ Crop Production and Biostimulation Laboratory, Université libre de Bruxelles, Brussels, Belgium. ✉email: david.cannella@ulb.be

The plant cell wall is a dynamic structure mostly made up of high molecular weight polysaccharides, i.e., cellulose, hemicellulose, pectin and the heteropolymer lignin¹. This complex aggregate confers structural integrity and physical protection to plant cells¹. To overcome the cell wall barrier, phytopathogens have developed an ingenious arsenal of enzymes collectively referred to as cell wall-degrading enzymes (CWDEs)². Thus, the structural cell wall integrity (CWI) is constantly monitored through dedicated molecular sensors and unique signaling mechanisms, including diffusible cell wall-derived molecules, i.e., oligosaccharides^{3–5}.

A novel family of CWDEs, the lytic polysaccharide mono-oxygenases (LPMOs), was discovered in 2010⁶, and despite its potential role in plant pathogenicity⁷, its biological significance in plant–pathogen interactions is still overlooked. LPMOs are metalloenzymes, bearing a mono-copper atom in a unique T-shape histidine-brace pocket that catalyzes the oxidative cleavage of 1,4 glycosidic bonds of polysaccharides, including cellulose, chitin, starch and xyloglucans⁸. The oxidative cleavage can take place at either C1- or C4-position of the pyranose ring. This cleavage yields a full array of oxidized and native cellulose- or cello-oligosaccharides (COS), i.e., glucose polymers of variable degrees of polymerization (DP from 2 to 10), as well as their C1- or C4-oxidized counterparts⁶. The catalytic mechanism, still under debate, depends on the presence of O₂ or H₂O₂ as electron sink for the redox activity; however, an external electron donor is always needed to cleave polysaccharides⁹. During *in vitro* tests, reductants such as ascorbate or gallate are often used to transfer electrons to LPMO. In addition, lignin-derived phenols^{10–12}, photoactivated pigments such as chlorophyllin^{9,13} and protein partners like cellobiose dehydrogenases (CDH)¹⁴, are all possible electron donors for LPMO *in vivo* activity¹⁵.

Widely distributed across the entire tree of life¹⁶, the LPMOs are particularly abundant in bacterial and fungal kingdoms¹⁷. According to the carbohydrate-active enzyme database (www.cazy.org), LPMOs are classified into seven “auxiliary activity” (AA) families: AA9–11 till AA13–16. The genome of several organisms (especially phytopathogenic fungi) features multiple LPMO gene copies. For example, *Fusarium graminearum* and *Botrytis cinerea* count, respectively, 13 and 10 AA9 isoforms¹⁸, a family generally active against cellulose and xyloglucans⁸. So far, none LPMO active on plant cell wall polysaccharides were found in the plant’s genome.

Plant cells possess at least three partially overlapping layers of defenses defined as pattern-triggered immunity (PTI), damage-triggered immunity (DTI), and effector-triggered immunity (ETI), which constitute the so-called plant immune system¹⁹. The ETI confers a robust resistance response, as it is initiated following recognition of pathogen virulence effectors (Avr-proteins) by plant cytoplasmic resistance genes (R-genes)²⁰. On the contrary, PTI triggers less powerful resistance responses as compared to ETI, but it provides broad-spectrum protection¹⁹. PTI is initiated upon recognition of evolutionary-conserved pathogen-associated molecular patterns (PAMPs), which are sensed by plants through a plethora of plasma membrane-anchored pattern-recognition receptors (PRRs)²¹. Similarly, plants can self-trigger DTI by recognizing damage-associated molecular patterns (DAMPs), which comprise cell wall-derived molecules as well as *de novo* synthesized stress-associated peptides^{19,22,23}.

Common signaling events underlying PTI/DTI involve Ca²⁺ influx into the cytoplasm²⁴, activation of mitogen-activated protein kinase (MPK) cascades²⁵, reactive oxygen species (ROS) accumulation²⁶, and an extensive transcriptional reprogramming including the expression of transcription factors (TFs)²⁷. During PTI/DTI, plants accumulate signaling hormones such as salicylic acid (SA), jasmonic acid (JA), and ethylene (ET), while several

hours after PTI/DTI activation, callose deposition occurs at the cell wall^{25,28}. Besides, PTI/DTI triggers the synthesis of a wide range of specialized metabolites including camalexin, an indolic phytoalexin that plays an essential role in plant resistance²⁹. Noteworthy, plant defenses are governed by spatial and temporal dynamics²⁷. For example, signaling events triggered by PAMP or DAMP perception occur within seconds to minutes, whereas transcriptome, cellular, and physiological responses are triggered within hours to days.

Thorough studies have investigated the elicitor properties of DAMPs derived from the hydrolysis of polysaccharides such as pectin and hemicellulose, i.e., oligogalacturonides (OGs)^{30,31} and xyloglucan³². More recently, the community started to investigate deeper structures of the plant cell wall. Cellulose-derived molecules, mainly cellobiose³³ and cellotriose³⁴ generated by glycoside hydrolase enzymes, were demonstrated to behave as DAMPs triggering plant immunity³⁵. On the other hand, little is known about the biological implications of oxidative deconstruction of cellulose conducted by AA enzymes, especially those belonging to the redox family of LPMOs. Although a hypothetical role in plant pathogenesis was speculated¹⁸, the biological effects of cellulose deconstruction via oxidative mechanism, their perception, and the triggered signaling remained so far an elusive idea.

In this study, the *TtAA9E* from the fungus *Thermothielavioides terrestris* was chosen as a representative member of the AA9 LPMO family to produce a pool of COS comprised of native and their C1- and C4-oxidized counterparts (hereafter named AA9_COS). We highlighted that AA9_COS treatment leads to a strong transcriptomic reprogramming in Arabidopsis, mainly associated with plant immunity. Together with other biotic stress responses, the antimicrobial phytoalexin camalexin markedly accumulated after AA9_COS treatment. Moreover, we identified two leucine-rich repeat (LRR)-receptor-like kinase (RLK) proteins, namely, *Stress Induced Factor 2* and *4*, crucial to signal the AA9_COS-dependent responses. Most importantly, a reduction of *B. cinerea* propagation was observed in AA9_COS-treated plants, paving a route for a biotechnological application for these molecules.

Results

AA9 genes of *B. cinerea* are expressed during plant infection and encode enzymes with putative C1/C4 regioselectivity as *TtAA9E*. In this work, we obtain oxidized COS from the conversion of cellulose using the *TtAA9E* enzyme produced by the fungus *T. terrestris* (Fig. 1). This family of enzymes is present on the necrotrophic pathogen *B. cinerea*, and they are selectively expressed during the infective process in Arabidopsis and none during growth on dextrose media (Supplementary Fig. 1). The *TtAA9E* enzyme feature a C1/C4 regioselectivity^{13,36} during the oxidative cleavage of the β-1,4-glycosidic bonds when incubated on the highly accessible phosphoric acid swollen cellulose (PASC) that was purposely chosen as the ideal substrate to ensure stable and sufficient amount of AA9_COS. The COS so obtained were purified with molecular filter (3 kDa cut-off), the absence of residual peptides was checked with sodium dodecyl sulfate-polyacrylamide gel electrophoresis (SDS-PAGE; Supplementary Fig. 2) and further characterized with high-performance anion-exchange chromatography with pulsed amperometric detection (HPAEC-PAD; Fig. 1a). The mixture of cellulose-derived COS presented both native COS and their aldonic C1-oxidized forms with various DP (DP2–7) with a slight enrichment toward cellobionic, cellotronic, and cellotetraonic acid compared to their native counterparts, whereas the C4-oxidized (gemdiol) COS although detected represented a very minor fraction of the entire mixture (Fig. 1a).

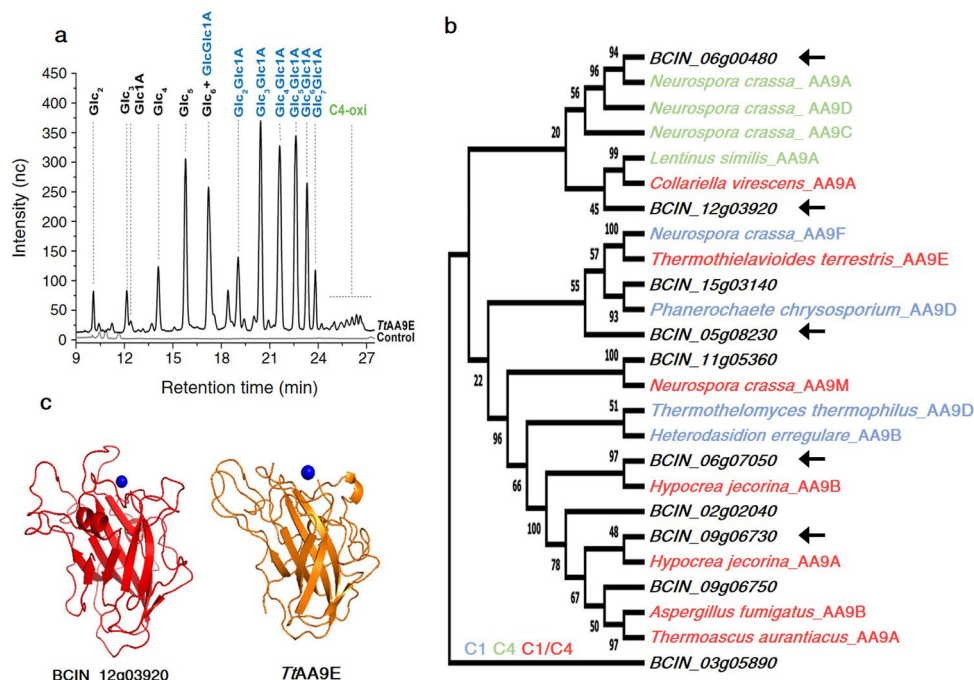


Fig. 1 *BcAA9s* sequence alignment, structural prediction, and *TtAA9E*-derived cello-oligosaccharide characterization. **a** HPAEC-PAD analysis of the products generated by *TtAA9E* using PASC 0.5% (w/v) as cellulosic substrate. The shown profile is the average of five independent experiments and relative chromatograms. Glc2 cellobiose, Glc3 cellobiose, Glc4 cellobiose, Glc5 cellopentaose, GlcGlc1A cellobionic acid, Glc2Glc1A cellobionic acid, Glc3Glc1A cellobionic acid, Glc4Glc1A cellopentaonic acid, Glc5Glc1A cellohexaonic acid, Glc6Glc1A celloheptaonic acid, Glc7Glc1A cellooctaonic acid. **b** Sequence-based comparison of *BcAA9s* with AA9 enzymes biochemically and structurally characterized. The phylogenetic tree was created based on the alignment of catalytic domain. Colors indicated the oxidative regioselectivity: C1, blue; C4, green; C1/C4, red; not characterized, black. The most expressed *BcAA9s* during *B. cinerea*-*Arabidopsis* interaction are labeled with arrows. **c** Structural comparison between *TtAA9E* and BCIN_12g03920 was built using the Swiss-Model Server and the *TtAA9E* crystal structure was obtained from the protein data bank (PDB:3EII). The structural models are shown in ribbon representation and copper ion is shown as a blue sphere.

Interestingly, a similar regioselectivity and structure was predicted from sequence alignment for some *B. cinerea* AA9s (*BcAA9*) and structurally resolved AA9s. In particular, the BCIN_12g03920 folding prediction showed a highly similarity in structure compared to *TtAA9E* (Fig. 1c). *BcAA9s* were already shown being expressed during necrotrophic growth in crops and fruits⁷, therefore we investigated whether also during *Arabidopsis* infection these could be expressed. The mRNA accumulation of the entire *BcAA9* gene family was measured 48 h after inoculation of *Arabidopsis* leaves (Supplementary Fig. 1). Five out of ten *BcAA9* genes showed substantial over-expression (fold change (FC) > 2) when compared to growth on dextrose medium. Among them, BCIN_12g03920 showed particularly high expression *in planta* (Supplementary Fig. 1). The phylogenetic tree in Fig. 1b comparing the *BcAA9s* catalytic domain sequences with structurally resolved AA9s enzymes showed three (BCIN_06g07050, BCIN_09g06730, and BCIN_12g03920) out of five *in planta*-expressed *BcAA9* genes clustering with AA9s enzymes from other species featuring C1/C4-regioselectivity.

Treatment with LPMO-generated COS protects plants against *B. cinerea*. Upon PTI or DTI activation, the plant defense responses follow distinct temporal activation dynamics²⁷; therefore, the most appropriate time point for the detection of each specific response was chosen accordingly. To evaluate whether treatments with AA9_COS conferred resistance toward phytopathogens, as previously demonstrated for pectin-derived OGs³⁷, we first performed a dose-response analysis of two defense marker genes 1 h after treatment. The *FLG22-INDUCED*

RECEPTOR-LIKE KINASE 1 (FRK1) and *WRKY DNA-BINDING PROTEIN 18 (WRKY18)* genes³⁸ showed a significant ($p < 0.05$) induction when plants were treated with 100 μ M AA9_COS (Supplementary Fig. 3). Therefore, rosettes of *Arabidopsis* plants were drop-treated with 100 μ M AA9_COS and inoculated with *B. cinerea* spore suspension (5×10^5 spores mL^{-1}) 24 h after AA9_COS treatment. Besides mock treatment, a solution containing an equimolar concentration of cellobiose was used as a positive control treatment³³. The *B. cinerea* necrotic lesion sizes were significantly ($p < 0.05$) reduced by 30% upon AA9_COS treatment when compared with mock-treated leaves (Fig. 2a, b). These data are in accordance with the *B. cinerea in planta* growth performed 3 days after infection, which highlighted a reduction in fungus growth of approximately 60% (Fig. 2c). On the other hand, a lower protective effect, in terms of lesion size and fungal *in planta* growth, was observed in *Arabidopsis* plants treated with 100 μ M cellobiose (Fig. 2a-c). Interestingly, similar protective effects of AA9_COS treatment against *B. cinerea* were observed in 2-month-old tomato plants (*S. lycopersicum* L.; Supplementary Fig. 4a, b).

Callose deposition is a typical response that plants deploy to reinforce the plant cell wall during pathogenic attack²⁷. To assess its deposition, leaves from 5-week-old *Arabidopsis* plants were stained with aniline blue 6 and 24 h following 100 μ M AA9_COS and 100 μ M cellobiose treatment (Fig. 2e). A substantial increase in callose accumulation was detected following AA9_COS treatment at both time points (Fig. 2d), while no callose spots were detected after cellobiose treatment (Fig. 2d, e and Supplementary Fig. 5a)³³. Interestingly, the dynamics and amplitudes in callose deposition due to AA9_COS treatment

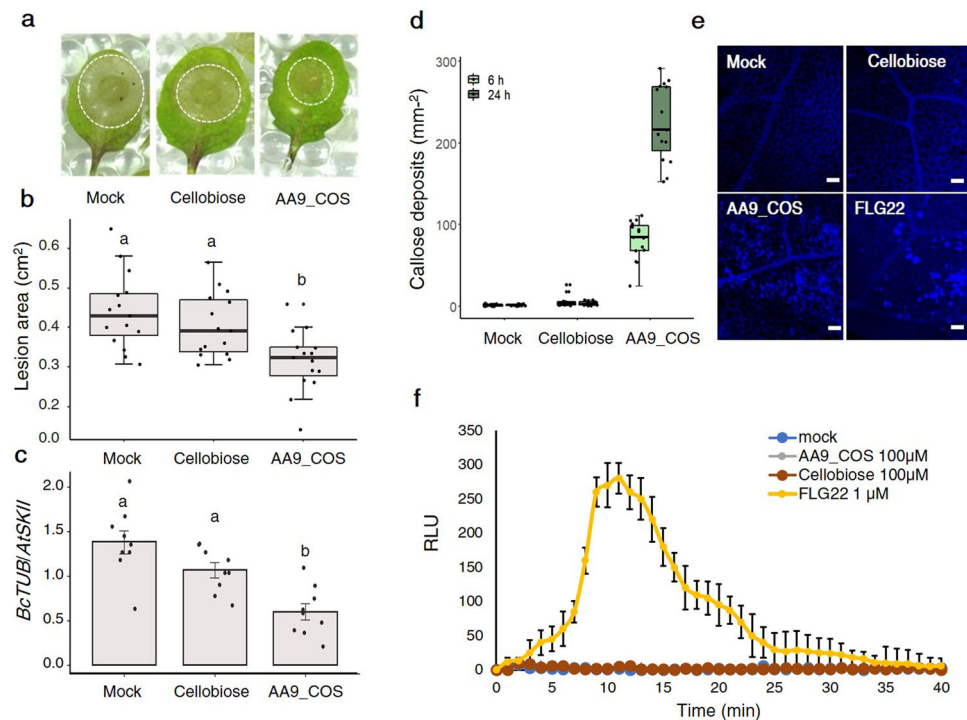


Fig. 2 AA9_COS induces DTI responses and protects against *B. cinerea*. **a** Five-week-old Arabidopsis plants were treated with 100 μ M cellobiose, 100 μ M AA9_COS, or mock, and 24 h later, detached leaves were spotted with 10 μ L spore suspension (5×10^5 spores mL^{-1}). Images were taken 3 days after infection and representative pictures are reported. **b** Box plots showing median value of the area of necrotic symptoms reported in **a**. Five leaves from three plants ($n = 3$) were analyzed. This experiment was repeated three times. **c** The *in planta* growth of *B. cinerea* was determined 3 days after infection by qRT-PCR using housekeeping genes specific for Arabidopsis (*AtSKII*) and *B. cinerea* (*BcTUB*). Data represent mean \pm SD of three independent experiments. **d** Five-week-old Arabidopsis plant leaves were treated with 100 μ M cellobiose, 100 μ M AA9_COS, or mock and callose was determined by aniline-blue staining 6 and 24 h after treatments. The values of quantification relative to five leaves from five individual plants ($n = 5$) for each treatment and time point were analyzed. This experiment was repeated three times. Callose deposition was revealed by using the ImageJ software and representative pictures are reported in **e**. **f** For each treatment, the luminol-based H_2O_2 detection was performed in 14-day-old Arabidopsis seedlings ($n = 10$) from 0 to 40 min after AA9_COS and cellobiose treatments. Values are shown as mean \pm SD. A representative experiment is shown in the figure. All the experiments were performed in three independent experiments with similar results. Lower case letters denote significant ($p < 0.05$) differences according to one-way ANOVA test with Tukey's post hoc multiple comparisons.

were proportional to time, acting stronger at 24 h than at 6 h (Fig. 2d, e and Supplementary Fig. 5a).

The transient and rapid generation of ROS is a hallmark of the response to microbe-associated molecular patterns (MAMPs) and chemical elicitor treatments^{26,39,40}. Hence, the short-term (0–40 min) H_2O_2 generation was evaluated by the luminol-based assay (Fig. 2f). Interestingly, no measurable short- and long-term H_2O_2 and O_2^- production (Supplementary Fig. 5b) was detected following AA9_COS treatment, indicating that AA9_COS triggers defense responses in a ROS-independent manner.

Transcriptomic analysis of AA9_COS-induced reprogramming in Arabidopsis. To gain insights into the dynamics of transcriptome reprogramming triggered by AA9-COS, Arabidopsis plants (14-day-old) were treated with (i) *TtAA9E* product mixture (AA9_COS), and compared with treatments using (ii) cellobiose, the only characterized cellulose-derived product eliciting plant defense; the experimental set was completed with (iii) mock treatments. To detect early responses⁴¹, the genome-wide transcriptomic analysis was performed 1 h after treatments using Arabidopsis 1.0 ST microarray chip (Affymetrix). Exogenous application of AA9_COS had a strong impact on the plant transcriptome landscape leading to changes in the expression of 545 genes (\log_2 FC > 1 or < -1), of which 482 genes were

upregulated and 63 genes were downregulated compared to mock-treated plants (Fig. 3a). Conversely, cellobiose treatment modulated 352 genes, of which 283 were upregulated and 69 were downregulated compared to mock-treated plants (Fig. 3a). A principal component analysis explained 53% of the combined variance and clearly separate mock-, cellobiose-, and AA9_COS-treated samples (Fig. 3b). To assess the microarray data reproducibility, quantitative real-time PCR (qRT-PCR) analysis was performed on ten different genes (Supplementary Fig. 6). Microarray and qRT-PCR data showed a high and significant correlation ($R^2 = 0.89$, false discovery rate (FDR) = 3.9×10^{-8} ; Supplementary Fig. 6). To identify the biological processes in which the AA9_COS-responsive genes were involved, Gene Ontology (GO) and pathway enrichment analyses were performed (Supplementary Data 1). Most of the detected GO terms were related to plant defense, including responses to bacterial and fungal attacks (Fig. 3c). Among the enriched categories in AA9_COS-treated plants, there are *Innate Immune regulation*, *Cell wall modulation*, *Signaling*, *Response to hormones*, and *Cell death regulation* (Fig. 3c). On the contrary, plants treated with cellobiose had the greatest enriched cluster associated solely with *Cell wall reorganization* (Fig. 3d). In summary, the enrichment analysis highlighted that the exposure of Arabidopsis to AA9_COS led to more complex and differential plant defense responses as compared to the cellobiose treatment.

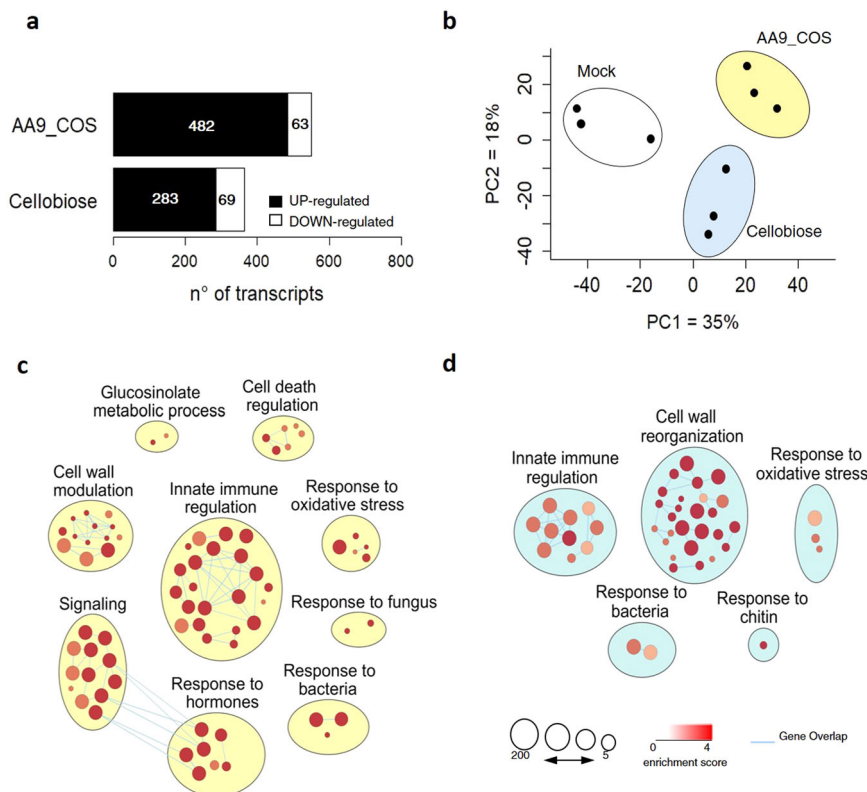


Fig. 3 Global analysis of early transcriptomic changes in *Arabidopsis* seedlings treated with AA9_COS and cellobiose. **a** Fourteen-day-old *Arabidopsis* seedlings were treated with 100 μ M AA9_COS, 100 μ M cellobiose, or mock; 1 h after treatment, 15 seedlings were pooled and flash-frozen in liquid nitrogen. Three independent pools ($n = 3$) for each treatment were produced and their relative transcriptome was analyzed. Genes featuring a \log_2 FC ≥ 1 or ≤ -1 compared to mock ($p \leq 0.05$) were considered as differentially expressed. **b** Principal component analysis of transcriptome responses induced by AA9_COS (pale yellow), cellobiose (pale blue), and mock treatment (gray). The overall gene expression similarities between samples are visualized using two principal components (PC1 and PC2), representing 35 and 18% of the total variation, respectively. **c, d** Gene Ontology (GO) enrichment analysis related to biological processes of 482 upregulated by AA9_COS (**c**) and 283 genes upregulated by cellobiose treatments (**d**). The GO analysis was performed by using the *g:Profiler* software (Benjamin-Hochberg FDR < 0.05) and the *EnrichmentMap* function of *Cytoscape*⁶⁰. Each node represents a pathway, edges represent overlapped genes between nodes, and circle size represents the number of genes encompassed.

LPMO-generated COS triggers powerful plant defense responses along with SA, JA, and ET hormone production.

To better understand the signaling events specifically induced by LPMO-derived products, we performed a hierarchical cluster analysis using AA9_COS and cellobiose transcriptome data. Clusters I and II were more responsive to AA9_COS than to cellobiose, whereas cluster III showed comparable gene expression between treatments (Fig. 4a and Supplementary Data 2). These clusters contained most of the core defensive marker genes like *FRK1*, *WRKY33*, and *NAC DOMAIN CONTAINING PROTEIN 55 (NAC055)*³⁸, as well as several genes encoding LRR-RLKs and wall-associated receptor kinases (Fig. 4b, c and Supplementary Data 2). Cluster IV contained a few genes showing enhanced expression in cellobiose-treated than in AA9_COS-treated plants (Fig. 4a). These genes are associated with carbohydrate transport (Supplementary Data 2). Regarding the genes modulated by both AA9_COS and cellobiose and treatments, we observed that 26% (158 genes) of the total upregulated genes were common between treatments, whereas the percentage decreased to 15.7% (18 genes) for the shared downregulated genes (Fig. 4d). Interestingly, the $-\log_2(\text{FDR})$ analysis showed that AA9_COS-induced genes were more enriched for SA- and JA-responsive genes as compared to the cellobiose-induced genes, whereas a slight enrichment of ET-responsive genes was detected (Fig. 4e). These predictions were further proved by liquid chromatography tandem mass spectrometry (LC-MS) quantification of SA and JA

and gas-laser detection for ET, relative to AA9_COS-treated plants (Supplementary Fig. 7). About fourfold and eightfold increase in SA and JA levels, respectively, were detected 24 h after AA9_COS treatment as compared to mock. Instead, the ethylene was monitored in a time-course analysis from the immediate applications of AA9_COS until the following 24 h. An early twofold increase of ET was observed 2 h after AA9_COS treatment as compared to mock and significantly higher ET level lasted till 4 h after treatment, which is typical for this volatile hormone²⁷ (Supplementary Fig. 7).

AA9_COS modulates biotic-associated TFs. The identification of TFs and their network is an important analysis for evaluating defense responses in expressomics data. Therefore, we performed a correlation network analysis (Pearson correlation > 0.9) using expression data with differentially expressed genes (DEGs) induced by AA9_COS treatment (\log_2 FC ≥ 1 ; Fig. 5). The analysis showed that WRKYs were the most represented TFs, followed by MYB, NAC, and ERF families (Supplementary Table 1). WRKY genes known to play a role in PTI were found as central hubs in the network (*WRKY48*, *47*, *11*, *72*, *18*, *29*, *30* and *33*), together with *WRKY22* and *25* that were not previously associated with biotic stress³⁸ (Fig. 5 and Supplementary Table 1).

Moreover, AA9_COS induced the expression of several NAC genes (such as *NAC47* and *55*; Fig. 5). In addition, members of

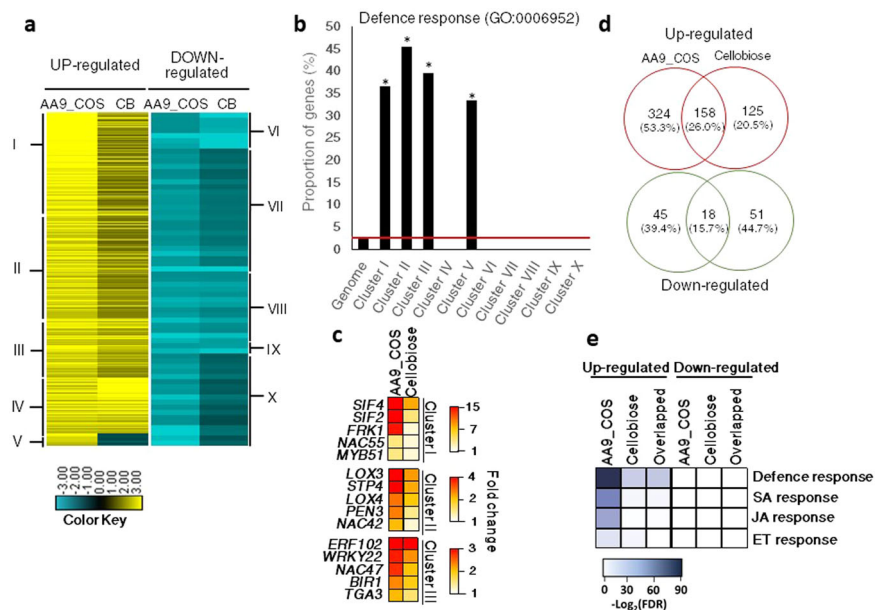


Fig. 4 Transcriptomic changes comparison between AA9_COS and cellobiose (CB) treatments. **a** Hierarchical clustering analysis of gene expression patterns that show significant expression changes as compared to mock (\log_2 FC ≥ 1 or ≤ -1 , $p \leq 0.05$) 1 h after 100 μ M AA9_COS or 100 μ M cellobiose treatments in 14-day-old Arabidopsis Col-0 plants. The clusters were divided into upregulated (yellow) or downregulated (blue) genes. **b** The proportion of genes associated with the defence response GO term (GO:0006952 Supplementary Data 3) was evaluated per cluster. **c** Heatmap of the selected defense genes belonging to clusters I-III. **d** Venn diagram shows specific and shared upregulated and downregulated genes induced by AA9_COS or cellobiose treatments. **e** The GO enrichment analyses performed with PSEA indicated that defense- and phytohormone-related genes were upregulated both by AA9_COS and cellobiose treatments (Supplementary Data 4). The color key represents the enrichment significance shown as $-\log_2(\text{FDR})$.

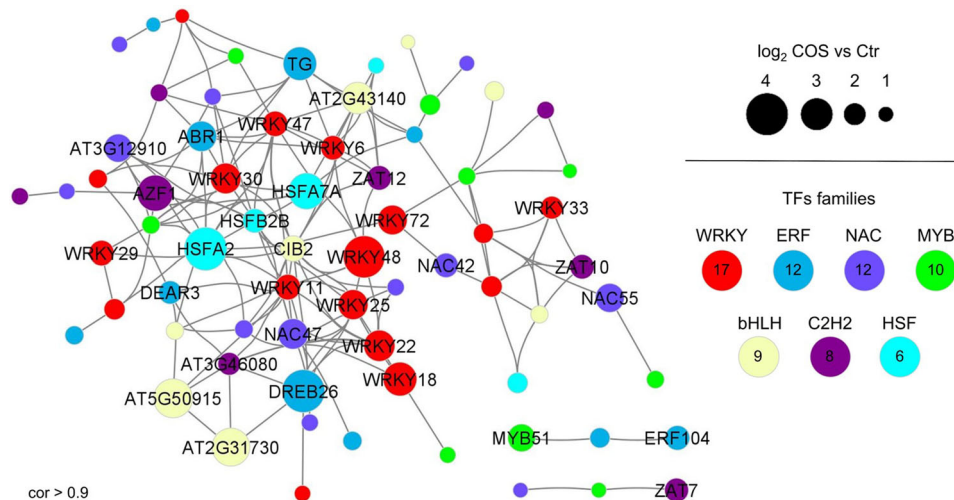


Fig. 5 Correlation network of AA9_COS-upregulated transcription factors (TFs). The correlation network was performed using significantly ($p < 0.05$) upregulated genes belonging to TF families. Gray edges indicate a positive correlation among TF genes, whereas the circle sizes represent the different magnitude of gene expression reported as \log_2 FC AA9_COS vs mock. Only co-expressed upregulated TFs with $r > 0.9$ and TF families with at least five members upregulated in AA9_COS were visualized in the network. The correlation network related to downregulated TFs is reported in Supplementary Fig. 8.

the MYB TFs family were either upregulated or downregulated by AA9_COS treatment (Fig. 5 and Supplementary Fig. 8). Among the MYBs upregulated by AA9_COS, we found MYB51 gene, a major regulator of the MAMP-dependent indole glucosinolate accumulation in Arabidopsis⁴². Besides the canonical defense-associated TFs, we also observed members of bHLH, C2H2, and HSF families being modulated by AA9_COS (Fig. 5). Interestingly, this analysis provided evidence that several marker genes are specifically enriched upon COS treatment probably indicating more suitable markers to evaluate native and oxidized COS immunity induction.

Carbohydrate transport proteins are specifically modulated by AA9_COS. Other classes worthy to be reported are those of sugar transporters such as sugar transport proteins (STPs), SWEET, and sucrose transport proteins (SUCs), well known to be hijacked by pathogens to favor sugar efflux from the cytosol to the apoplast^{43,44}. Several genes encoding sugar importer proteins such as STP-4, -13, and -1 were induced by AA9_COS mixture. On the contrary, genes encoding the most important SWEET bidirectional transporters (*SWEET 2*, *16*, *17*), involved in sugar export from the cytoplasm to the apoplast, were downregulated by treatment (Supplementary Table 2). These data suggest that

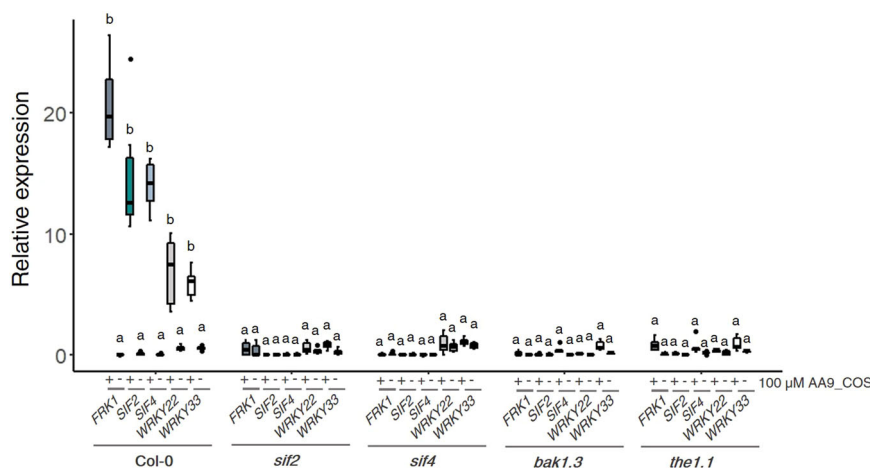


Fig. 6 Involvement of selected RLK receptors in signaling the AA9_COS-dependent defense gene expression. The expression of defense marker genes was evaluated in *sif2*, *sif4*, *bak1.3*, and *the1.1* loss-of-function Arabidopsis seedlings. Fourteen-day-old seedlings were treated with or without 100 μ M AA9_COS and qRT-PCR was carried out 1 h after treatment. Median values are plotted in the boxes with data generated from three independent pools ($n = 3$) of 15 seedlings each. One-way ANOVA test was performed; lower case letters denote significant ($p < 0.05$) difference between mock- and AA9_COS-treated plants.

AA9_COS might also counteract the pathogen invasion by leading plants to sequester edible resources for phytopathogens.

STRESS INDUCED FACTOR 2 and 4 and other LRR-RLKs regulate the AA9_COS-induced defense gene expression. To further decipher the molecular mechanism underlying defense activation by AA9_COS, the transcriptomic data were screened for PRRs and RLK proteins, pivotal players in DAMPs signaling²¹ (Supplementary Table 2). Two genes encoding LRR-RLKs, namely, *STRESS INDUCED FACTOR 2* and *4* (*SIF2*, *SIF4*), were strongly upregulated by AA9_COS and represented in cluster I (Fig. 4c). In addition, two other RLKs, such as *BRI1-ASSOCIATED RECEPTOR KINASE 1* (*BAK1*) and *THESEUS 1* (*THE1*), key players for flagellin perception²² and CWI sensing⁴, respectively, were triggered by AA9_COS (Supplementary Table 2) and selected for further studies. To evaluate the potential role played by these LRR-RLKs in signaling the AA9_COS-dependent defense gene expression, the *sif2*, *sif4*, *bak1*, and *the1* knockout (KO) mutants were treated with 100 μ M AA9_COS. The expression levels of three defense marker genes, *FRK1*, *WRKY22*, and *33*, along with *SIF2* and *SIF4* genes, were evaluated 1 h after treatment (Fig. 6). Interestingly, in all the AA9_COS-treated mutant lines, the expression of *FRK1* and *WRKY22* was equal to mock-treated Col-0 plants (Fig. 6). A slight but not significant increase in *WRKY33* expression was detected in AA9_COS-treated *sif2*, *bak1*, and *the1* KO lines as compared to mock-treated plants. However, the level of expression of these genes in the mutant background was substantially lower as compared to what observed in AA9_COS-treated Col-0 plants (Fig. 6). Altogether, these data suggest that these *BAK1* and *THE1* plasma membrane-localized RLKs might interact singularly or in combination with *SIF2* and/or *SIF4* to create an active complex for the perception of AA9_COS.

STRESS INDUCED FACTOR 2 and 4 regulate the AA9_COS-induced camalexin accumulation independently to MPK3/6 phosphorylation. The tryptophan-derived camalexin is a well-known antimicrobial metabolite produced by plants during pathogenic infection, i.e., *B. cinerea*^{29,45,46}. Camalexin was quantified in 14-day-old Col-0, *sif2*, and *sif4* KO mutants 24 h after 100 μ M AA9_COS, 100 μ M cellobiose, or mock treatments. The latter two yielded comparable levels of camalexin

(mock = 2.4 ± 1.4 ng g⁻¹, cellobiose = 3.7 ± 1.8 ng g⁻¹), whereas AA9_COS yielded 35.0 ± 5.4 ng g⁻¹ in Col-0 plants. On the contrary, no camalexin production, along with an increase of *B. cinerea* in planta growth, was observed in both *sif2* and *sif4* AA9_COS-treated plants (Fig. 7a and Supplementary Fig. 9). Given the involvement of the *MPK3-MPK6-WRKY33* module in the activation of the camalexin biosynthetic pathway⁴⁷, the expression of these genes was measured in Arabidopsis Col-0 plants 1 and 24 h after treatment with 100 μ M AA9_COS or 100 μ M cellobiose. Generally, treatments with AA9_COS yielded stronger inductions: 1 h after treatment a significant ($p < 0.05$) induction of *MPK3/6*, *WRKY33*, *PAD3*, and *PEN3* was detected, while at 24 h after treatment only *MPK3* gene was maintained expressed (Fig. 7b relative to 14-day-old plants). Instead for cellobiose treatment, a lower induction was observed: except for *MPK3/6*, at 1 h after treatment a slight expression was observed for *WRKY33*, *PAD3*, and *PEN3* genes as compared to mock-treated plant, whereas no significant ($p > 0.05$) differences were detected at 24 h (Fig. 7b). Finally, similar trends of *MPK3/6* and *WRKY33* gene expression were observed when comparing 2-week-old with 5-week-old plants (Supplementary Fig. 10). Moreover, the *MPK3/6* gene expression activation was completed by immunoblotting analysis. Early *MPK3/6* phosphorylation was detected after 100 μ M AA9_COS treatment, whereas no phosphorylation was observed upon treatments with 100 μ M cellobiose in Col-0 plants (Fig. 7c and Supplementary Fig. 12). Therefore, the *MPK3/6* proteins and their phosphorylated forms (p*MPK3/6*) were hybridized in Col-0, *sif2*, and *sif4* mutant lines. After AA9_COS treatment, we observed a signal for the p*MPK3/6* both in Col-0 and *sif2* and *sif4* KO lines, even if a slight decrease in p*MPK3/6* forms was observed in *sif4* KO lines (Fig. 7c and Supplementary Fig. 12). Altogether these data indicate the *SIF2/4* LRR-RLKs as key regulators to signal the AA9_COS-dependent response activation.

Discussion

In this study, we found that the mixtures of oxidized and native COS produced by the fungal cellulose-oxidizing LPMO AA9 enzyme (AA9_COS) are eliciting plant immune responses to higher and complete extent than the sole cellobiose, a native COS released instead by glucosyl hydrolase enzymes (hydrolytic CWDEs). The LPMO-driven oxidation of cellulose generates a mixture of C1- and

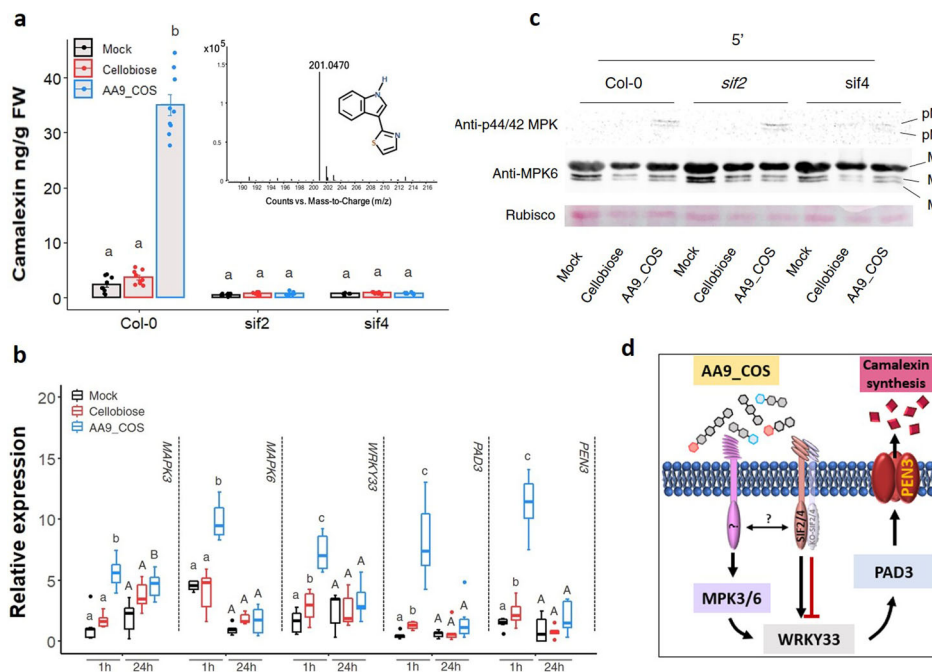


Fig. 7 AA9_COS induces camalexin biosynthesis and requires SIF2 and SIF4 LRR-RLK genes. **a** Camalexin was quantified in 14-day-old Col-0, *sif2* and *sif4* Arabidopsis seedlings by LC-MS 24 h after 100 μ M AA9_COS and 100 μ M cellobiose treatments. Bar plots represent the mean \pm SD of data generated from three independent experiments ($n = 3$). One-way ANOVA with Tukey's post hoc multiple comparisons ($p < 0.05$) were performed; lower case letters denote differences. The mass of camalexin is reported. **b** The expression of genes involved in camalexin signaling and biosynthesis was evaluated in 14-day old Col-0 Arabidopsis seedlings 1 and 24 h after 100 μ M AA9_COS, 100 μ M cellobiose, and mock. Median values are plotted in the boxes with data generated from three independent pools ($n = 3$). Each pool consisted of 15 seedlings. One-way ANOVA with Tukey's post hoc multiple comparisons ($p < 0.05$) was performed; lower case and capital letters denote difference at 1 and 24 h following treatments, respectively. **c** Immunoblotting analysis showing the early activation of MPK3 and MPK6 protein kinases after the indicated treatments. Fourteen-day-old Col-0, *sif2*, and *sif4* Arabidopsis seedling were treated with 100 μ M AA9_COS, 100 μ M cellobiose, and mock, and samples were collected 5 min after treatment. Western blot analysis was carried out using the following antibodies: anti-p44/42 MPKs antibody (Cell Signaling Technology, active forms) and anti-MPK6 (Sigma, total proteins), which recognized also the MPK3 and MPK4. Loading proteins were detected using the Ponceau S staining and Rubisco is shown in the bottom panel. Three independent experiments were performed with similar results. **d** Proposed model for the AA9_COS regulation of camalexin biosynthesis and signaling.

C4-oxidized and native COS (Fig. 1a), which leads to a wide transcriptome reprogramming and activation of immune responses in Arabidopsis (Figs. 4, 5, and 7). We observed that the AA9_COS-dependent defense response activation conferred increased resistance to the necrotrophic phytopathogens *B. cinerea* both in Arabidopsis and tomato plants (Fig. 2 and Supplementary Fig. 4). Additionally, we discovered that two plant LRR-RLKs, namely, SIF2 and SIF4, are required to fully signal the AA9_COS-dependent responses (Fig. 6), pointing toward their possible role in sensing biotic or abiotic stresses or, alternatively, DTI and CWI maintenance mechanisms. As indicated previously, DTI activation and CWI sensing are two distinct mechanisms implicated in monitoring chemical and mechanical alterations of the cell wall. Nevertheless, the partially overlapped pathways controlling these two mechanisms make it hard to distinguish one from another^{3–5}. In plant–pathogen interactions, the role of DAMPs resulting from the activity of hydrolytic enzymes on pectin and hemicelluloses is well established^{30,31}. Classic examples are the well-characterized pectin-derived OGs and xylans from hemicelluloses^{31,32,41,48}. Conversely, little is known about the signaling pathways and defense responses triggered by perturbations of the main load-bearing component of the cell wall, i.e., cellulose.

Fungal LPMOs possess the unique feature to not only produce diffusible DAMP signals in the form of peculiar mixtures of native, C1-, and/or C4-oxidized oligosaccharides but also to weaken the crystalline regions of the cell wall, causing loss of structural integrity^{8,49}. Indeed, LPMOs have been recently proposed to act earlier than other CWDEs during cellulose

degradation¹⁸, hence in light of the results presented here, it might play a pivotal role in plant–pathogen interactions. Previously, it was revealed that, during pathogenicity on different hosts, the necrotrophic fungus *B. cinerea* deployed three LPMOs, all from the AA9 subfamily⁷. In this work, we studied the transcription pattern of the entire *BcAA9* gene family during the infection of Arabidopsis plants by *B. cinerea* (Supplementary Fig. 1). The sequence alignment of the *BcAA9* catalytic domains against structurally resolved fungal AA9s enzymes showed that the majority of expressed proteins potentially have C1/C4 oxidative activity (Fig. 1b). Therefore, the *TtAA9E* from the saprophytic fungus *T. terrestris* was chosen from our collection to produce a representative AA9_COS mixture (containing either native and C1 and/or C4 oxidized COS) as predicted by the phylogenetic tree analysis related to *BcAA9* genes (Fig. 1b) and Supplementary Fig. 1). The mixture so produced (AA9_COS) contained native and oxidized (aldonic acids and gemdiols) oligosaccharides of various DP. Indeed, the LPMO-derived products, rather than the single native oligosaccharide, better represent the blend of COS released from the plant cell wall polysaccharides naturally occurring in a pathogenic attack. Therefore, the study of this more complex blends of COS provides a valuable biological output that was further characterized in the rest of the work.

In the graphical model (Fig. 8), we summarized all the major results obtained here from the transcriptomic reprogramming and cellular and physiological changes that conferred Arabidopsis higher resistance to the pathogenic fungus *B. cinerea* upon

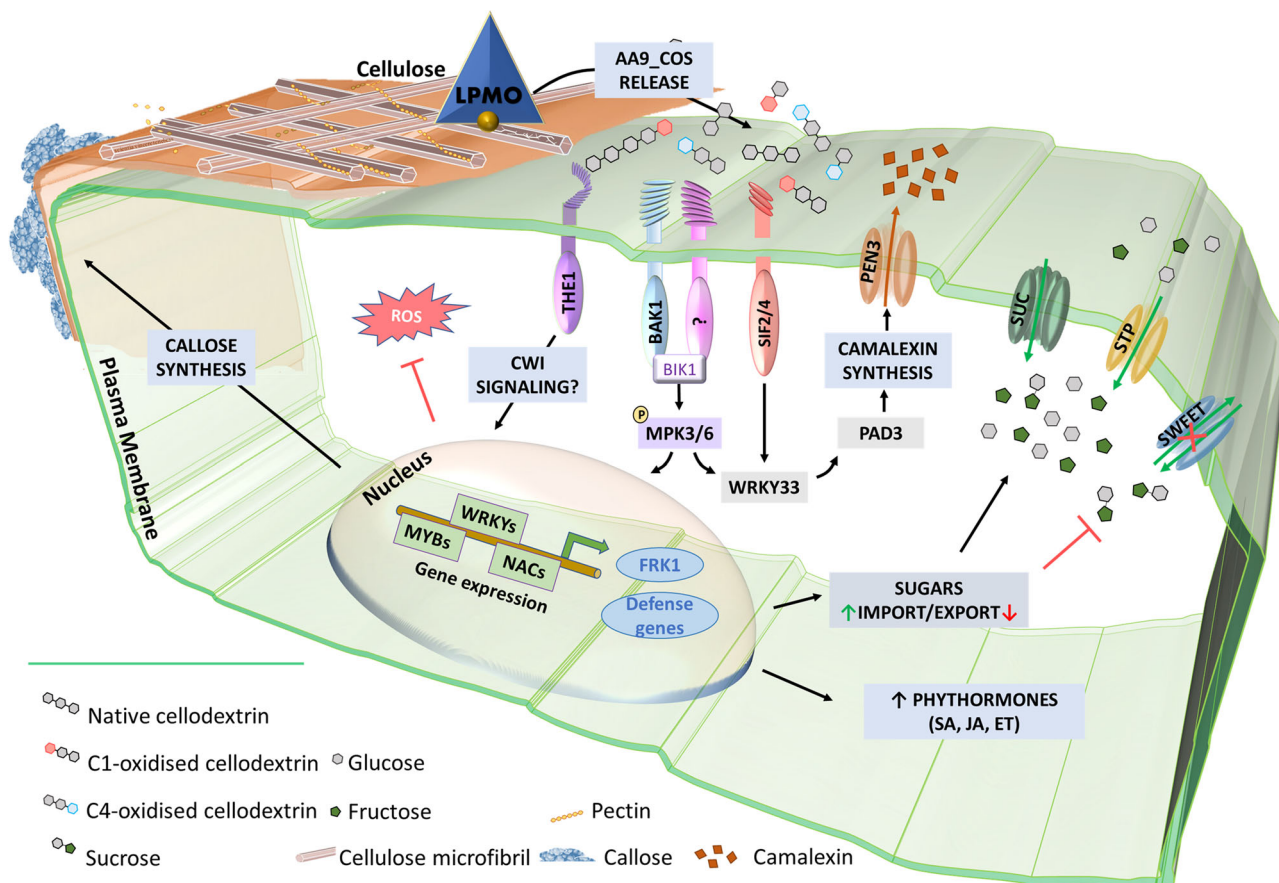


Fig. 8 Schematic model for AA9_COS perception, signaling, and defense responses in Arabidopsis. The degradation of plant cell wall polysaccharides by microbial LPMOs leads to the release of native and oxidized cello-oligosaccharides, such as AA9_COS. In the apoplast, plasma membrane-anchored PRR proteins, i.e., SIF2/4, BAK1, and THE1, after DAMP sensing activate ROS-independent DTI responses, which include callose deposition and phytohormone accumulation. Consequently, the recognition of AA9_COS induces a deep transcriptional reprogramming, including TFs belonging to the WRKY, MYB, and NAC families, as well as the phosphorylation of MPK3 and MPK6. This, in turn, leads to a remarkable synthesis of camalexin. Additionally, genes encoding for sugar transporters are modulated by AA9_COS treatment, with the induction of cytoplasmic sugars import (SUC and STP) and the inhibition of SWEET transporters involved in sugar export from the cytoplasm to the apoplast.

AA9_COS treatments. Several PRRs and RLKs were modulated by AA9_COS treatment (Supplementary Table 2) and the genes encoding two LRR-RLKs, *SIF2* and *SIF4*, were highly expressed (Fig. 4c and Supplementary Table 2). *SIF2* interacts with the FLS2-BAK1 PRR complex and regulates MAMP-dependent PTI pathway, involving MPK kinases, WRKY TFs and *FRK1* and pathogen-dependent stomata closure^{50,51}. Moreover, through a meta-data analysis, we recently identified *SIF4* as constantly expressed during several combined biotic and abiotic stress conditions⁵². In the results presented here, we showed that both *SIF2* and *SIF4* play a crucial role in signaling the AA9_COS-dependent responses such as camalexin production (Fig. 7a, d). Moreover, necrotrophic growth of *B. cinerea* was considerably higher in *sif2* and *sif4* KO mutants if compared to Col-0 plants probably due to a lesser amount of camalexin being produced in the mutants. Moreover, treatments with AA9_COS could still aid the plants against the pathogen in retarding its growth although only partially (Supplementary Fig. 9). Indeed, the MPKs gene expression and phosphorylation were rapidly triggered by AA9_COS treatment (Fig. 7b, c), which is in agreement with what was previously observed following OGs and native COS treatments⁵³ triggering camalexin⁵⁴ production and enhancing resistance to the fungus *B. cinerea*³⁷. The production of the antimicrobial compound camalexin is therefore the final output of defense mechanisms deployed by plants upon metabolic

reprogramming involving several anabolic enzymes²⁷. Our results showed the induction of key regulatory genes as well as the actual synthesis of this metabolite in AA9_COS-treated plants (Fig. 7a, b). Moreover, a vast de novo deposition of callose conferring resistance to *B. cinerea* (Fig. 2d, e) was observed. In contrast, these basal defenses were not triggered by cellobiose alone (Fig. 2d, e)³³. Interestingly, no expression of three PTI marker genes, as well as a null accumulation of camalexin, was detected in both *sif2* and *sif4* KO mutants after AA9_COS treatment (Figs. 6 and 7a), indicating these LRR-RLKs as potential key players for AA9_COS-regulated defense induction⁵⁰. Furthermore, only a slight decrease in MPK3/6 phosphorylation was observed in *sif4* mutants upon AA9_COS treatment as compared to wild-type plant (Fig. 7c). This is in accordance with previous data showing that, in *sif2* mutants, the MPK3/6 cascade is not impaired upon *Pst* DC3000 infection⁵⁰, suggesting that these two RLKs might regulate basal defenses in an MPK3/6-independent manner. Interestingly, a null AA9_COS-dependent *FRK1*, *WRKY22*, and *WRKY33* gene expression was observed in *bak1* and *the1* loss-of-function mutants, impaired for the membrane receptors required for flagellin²² and CWI sensing^{3,4}, respectively (Fig. 6). These results suggest that AA9_COS mixture might play a role also in signaling mechano-derived damages of cell wall⁵⁵, like those caused by abiotic stress, besides canonical immune responses.

gene expression induced by our mixtures, plants were treated 3 h after light onset, and samples were collected at the middle of the light period (steady state for metabolism).

For the *in planta* growth test of *B. cinerea*, 5-week-old Col-0, *sif2*, and *sif4*, and 2-month-old tomato plants were germinated in soil and grown in a controlled chamber (same growth conditions as above). Fifteen leaves from three independent plants were treated by applying 40–50 μL of filtered solutions per leaf. At the indicated time points, treated leaves were inoculated with 10 μL droplet of *B. cinerea* spores (5×10^5 spores mL^{-1}), and 3 days after infection, leaves were pooled, flash-frozen in liquid nitrogen, and stored at -80°C . Genomic DNA from ground-frozen samples was extracted and fungal biomass was quantified by qRT-PCR analysis using primers specific for *B. cinerea* (*BcTub*) and Arabidopsis (*AtSK11*)³⁷. Three independent pools ($n = 3$) were so replicated.

The *B. cinerea* symptomatology was performed in 5 detached leaves collected from three 5-week-old Arabidopsis or 2-month-old tomato plants ($n = 3$) by inoculating 10 μL droplet (5×10^5 spores mL^{-1}) per leaf. Three days after fungus inoculation, pictures were taken with a photo camera and the areas of the developing necrotic lesions were analyzed by the ImageJ software. This experiment was repeated three times.

The *B. cinerea* B05.10 strain was grown on potato dextrose agar medium at 21°C , with a photoperiod of 12 h light ($100 \mu\text{mol photons m}^{-2} \text{s}^{-1}$)/12 h darkness.

Sequence alignment, phylogenetic analysis, and structural model. The annotated AA9s from *B. cinerea* BCIN_15g03140, BCIN_05g08230, BCIN_06g00480, BCIN_12g03920, BCIN_03g05890, BCIN_11g05360, BCIN_09g06750, BCIN_09g06730, BCIN_02g02040, and BCIN_06g07050 were aligned with the AA9s biochemically and structurally characterized AfAA9B (PDBid 5X6A), CvAA9 (PDBid 5NLT), HjAA9A (PDBid 5O2W), HiAA9B (PDBid 2VTC), LsAA9A (PDBid 5ACF), MIAA9D (PDBid 5UFV), NcAA9A (PDBid 5FOH), NcAA9C (PDBid 4D7U), NcAA9F (PDBid 4QI8), NcAA9M (PDBid 4EIS), PcAA9D (PDBid 4B5Q), TaAA9A (PDBid 2YET), and TtAA9E (PDBid 3EII) using MUSCLE⁵⁷. Phylogenetic analysis was performed with the MEGA software⁵⁸ version 10.1.7 using the neighbor-joining method. The consensus tree was inferred using a bootstrap of 1000 replicates. The structural model of BCIN_12g03920 was generated using the Swiss-Model Automated Comparative Protein Server and using LsAA9A (PDBid 5ACF) as template. Protein structures were visualized with PyMol Molecular Graphics Systems (Version 1.5.0.4 Schrödinger, LLC, New York, NY, USA).

RNA extraction, cDNA preparation, and qRT-PCR analysis. Total RNA was extracted from 100 mg of ground-frozen samples using the Spectrum™ Plant Total RNA Kit (Sigma-Aldrich), and the RNA purity was determined through NanoDrop 2000 UV-Vis Spectrophotometer (Thermo Scientific, Loughborough, UK). First-strand cDNA was synthesized by using SOLIScript RT cDNA synthesis MIC (Solis Biodyne) and qRT-PCRs were performed using SYBR Selected MasterMix 2 \times (HOT FIREPol® SolisGreen® qPCR Mix, Solis Biodyne), following the manufacturer's protocol in a MyiQ real-time PCR detection system (Biorad). The cycling conditions consisted of an initial 7 min at 95°C , followed by 40 two-step cycles at 95°C for 5 s and 60°C for 30 s. Melting curve analysis was performed after cycle completion to validate amplicon identity. Relative expression levels for plant gene expression were calculated following the standard curve-based method by using *ACTIN2* and *Elongation Factor-1 α* as reference genes⁵⁹. Relative expression levels for *B. cinerea* AA9 genes *in planta* and in PDA medium growth were calculated following the standard curve-based method by using *BcTUB* as reference gene. Gene-specific primers used in this work are listed in Supplementary Table 3. All the qRT-PCRs were measured twice from 3 independent ($n = 3$) pools each consisting of 15 leaves.

Microarray hybridization and data analysis. RNA sample preparation for microarray hybridization was carried out as described in the Applied Biosystems™ GeneChip™ Whole Transcript (WT) PLUS Reagent Kit User Guide (Thermo Fisher Scientific, Waltham, MA, USA). Briefly, 200 ng of total RNA was used to generate double-stranded cDNA. Twelve micrograms of subsequently synthesized cDNA was purified and reverse transcribed into single-stranded cDNA (sscDNA), where unnatural dUTP residues were incorporated. Purified and labeled sscDNAs were hybridized to Arabidopsis Gene 1.0 ST arrays (Affymetrix), and the fluorescent signals were measured with an Applied Biosystems™ GeneChip Scanner 3000 7G System. Three biological replicates were hybridized for AA9_COS, cellobiose, and mock-treated RNA samples extracted from three independent pools ($n = 3$) for each treatment consisting of 15 seedlings per pool. Sample processing was performed at a Genomics Core Facility, “KFB—Center of Excellence for Fluorescent Bioanalytics” (Regensburg, Germany). Normalized probe set signals in the log₂ scale were calculated by using the RMA algorithm (Applied Biosystems GeneChip Expression Console v1.4 software) and the DEGs were selected using two criteria: log₂ FC ≥ 1 or ≤ -1 and Student's *t* test *p* value ≤ 0.05 . Average linkage hierarchical clusters of DEGs were generated by using Cluster 3.0 and visualized by Java Treeview.

GO, pathway enrichment analysis, and network analysis. GO analysis related to the biological process was performed by the Cytoscape software using upregulated

genes (log₂ FC > 1 , $p < 0.05$) through the g:Profiler software using Benjamini and Hochberg FDR (< 0.05) as filtering step accordingly to refs. ^{60,61}. In addition, to better visualize the results of the GO analysis, terms were clustered by using the “Autoannotate” in Cytoscape tool, thus obtaining 10 clusters associated with defense responses. The network analysis was performed using the “Expression Correlation” app of Cytoscape software⁶².

Callose staining. Callose deposit quantification was performed following ref. ³⁹. Briefly, for each treatment 5 leaves from five 5-week-old Arabidopsis plants were analyzed ($n = 5$). This experiment was performed three independent times. Leaves were stained using 0.01% (w/v) aniline blue in 150 mM K₂HPO₄ (pH 9.5) buffer for 30 min and then de-stained in a lactophenol clearance solution overnight. Leaves were examined by stereofluorescence microscopy with an Azio Zoom V.16 (Carl Zeiss Inc., Oberkochen, Germany) and callose spots were quantified using the ImageJ software. All staining experiments were repeated three times and representative images were selected.

Hydrogen peroxide detection assays. Hydrogen peroxide (H₂O₂) was assayed with Arabidopsis plant cultivated in vitro or in soil. The H₂O₂ in situ detection was performed following ref. ⁶³. Briefly, for each treatment, 10 leaves from 3 5-week-old Arabidopsis plants were droplet-treated (40–50 μL per leaf) with the indicated compounds. At 24 h after treatment, leaves were gently vacuum-infiltrated (5 min) with 1 mg mL^{-1} 3,3'-diaminobenzidine (DAB) dissolved in 10 mM sodium phosphate buffer and 0.05% (v:v) Tween 80. The staining reaction was terminated 5 h after DAB infiltration, and leaves were fixed in ethanol:glycerol:acetic acid 3:1:1. Chlorophyll was removed by several washing steps with 70% (v:v) ethanol, and pictures were taken with a stereomicroscope (Discovery V8, Zeiss).

Elicitor-induced H₂O₂ was also detected by luminol-peroxidase-based. Briefly, 20 leaves from 10 14-day-old Col-0 seedlings were cut and incubated in ddH₂O overnight. Also discs from 5-week-old Arabidopsis were cut and assayed similarly. Time-course luminescence was evaluated using the SpectraMax iD3 Multi-Mode Microplate Reader (Molecular devices) with an integration time per well of 1 s following application of the indicated compounds.

Superoxide detection assay. Superoxide anion (O₂⁻) was assayed by performing nitro blue tetrazolium (NBT) assay⁶³. Briefly, for each treatment, 10 leaves from 3 5-week-old Arabidopsis plants were droplet-treated (40–50 μL per leaf) with the indicated compounds. At 24 h after treatment, leaves were cut and placed in tubes containing the NBT solution (3.5 mg mL^{-1} NBT, 50 mM sodium phosphate buffer, pH 7.5) and subjected to vacuum infiltration for 5 min. Then leaves were incubated under dark conditions overnight. Chlorophyll was removed by several washing steps with 70% (v:v) ethanol, and pictures were taken with a stereomicroscope (Discovery V8, Zeiss).

LC-MS for camalexin quantification and hormones. For each treatment, camalexin was extracted from a pool of 15 seedling of 14-day-old Arabidopsis, following method described in ref. ³⁷. Briefly, 100 mg of ground-frozen samples were soaked using 80% (v:v) methanol in 1:1 (m/v) ratio. After homogenization, the supernatant was recovered through centrifugation at $17,000 \times g$ for 5 min and evaporated at 50°C in nitrogen gas atmosphere. The residues were finally resuspended in high-performance LC-grade methanol and filtrated with 0.22- μm filters. Each pool was then analyzed three times by LC-MS, a 1200 series rapid resolution LC system coupled to a 6520 series electrospray ionization (ESI)-quadrupole time-of-flight (QTOF) high-resolution mass spectrometer from Agilent Technologies (Waldbronn, Germany). The compound separation was performed using a reverse-phase LUNA® Omega 5 μm Polar C18 column ($250 \times 4.6 \text{ mm}$). The mobile phases were composed of 0.1% in water (solvent A) and acetonitrile (solvent B). The applied gradient was as follows: 0–2 min, 10% B; 2–13 min, 10–98% B; 13–23 min, 98% B; 23–25 min, 98–10% B; 25–30 min, 98% B; post-run 1 min. Data acquisition and analysis were carried out by the MassHunter Acquisition® software for QTOF (Version B.08), MassHunter Qualitative Analysis® (Version B.07) software, and MassHunter Quantitative Analysis® (Version B.07) software (Agilent Technologies). Three independent experiments/pools were prepared ($n = 3$) for each treatment.

Detection and quantification of JA and SA were performed at the Plant Observatory-Chemistry and Metabolomics platform (IJPB/INRA, Versailles, France)³⁹. Twenty-four hours after treatments with the indicated compounds, 15 leaves from three 5-week-old plants were immediately harvested, frozen, and ground in liquid nitrogen and stored at -80°C . Harvested material was extracted with 3 mL of acetone/water/acetic acid (80/19/1, v:v:v) and injected in high-performance LC-ESI tandem MS³⁹. Three independent pools ($n = 3$) were extracted.

Protein extraction and immunoblotting. For MPK3/6 immunoblotting, 15 seedlings 14-day-old Col-0, *sif2*, and *sif4* were treated with 100 μM AA9_COS, 100 μM cellobiose, or mock. Leaves were collected 5 min after treatment, immediately frozen in liquid nitrogen, and stored at -80°C for analysis. Proteins extraction and western blot analysis were performed following⁶⁴. Briefly, following protein extraction and fluorometric quantification (Qubit Protein Assay Kit, Thermo-fisher), 20 μg of proteins were denatured at 95°C for 10 min in SDS-PAGE loading

buffer and protein samples were separated on 12% acrylamide/bis-acrylamide SDS-PAGE gels. The separated proteins were transferred on a 0.45- μ m Immobilon-P PVDF membrane (Millipore). Blocking was performed in TBST containing 5% non-fat dry milk, and blots were incubated overnight at 4 °C with anti-A α MPK6 (Sigma), and anti-Phospho-p44/42 MPK (Thr₂₀₂/Tyr₂₀₄) (Cell Signaling Technology, antibody #9101), washed in TBST, and incubated with the secondary antibody anti-Rabbit IgG conjugated with horseradish peroxidase (HRP) enzyme (Promega) diluted to 1/10,000. The chemiluminescent detection of HRP was performed with Clarity™ Western ECL Substrate (Biorad) and ChemiDoc™ MP Imaging System (Biorad).

Ethylene emanation. Hundred seedlings of *Arabidopsis* Col-0 were cultivated in vitro during 14 days in square plates (12 × 12 cm) as described in ref. 65. Treatments were performed by spraying 100 μ M AA₉-COS and 100 μ M cellobiose or mock and a total of 8 plates ($n = 8$) were measured. Ethylene production was analyzed with the ETD 300 detector (Sensor-Sense, Nijmegen, the Netherlands). A valve control box allowed automated sampling of ethylene production by six plates at a time, sequentially under a stop-and-flow routine where the gas from one plate accumulated during 1 h, and then flushed to the detector for 12 min; the first sampling relative to the first hour is omitted due to technical cell mounting after spraying the samples. The measurements were then performed over a continuous period of 24 h for each plate.

Statistics and reproducibility. Data shown in graphs are presented either as the mean with S.D. or as median values from three biological replicates as indicated in the figure captions. Statistical significance was tested by one-way analysis of variance (ANOVA) test to compare treatments with mock (asterisks denote significant difference, $p < 0.05$), whereas one-way ANOVA test followed by Tukey's post hoc test was performed to compare different treatments to each other and mock (different letters indicate significant differences, $p < 0.05$). Student's t test ($p < 0.05$) was used to identify DEGs from transcriptome data.

Reporting summary. Further information on research design is available in the Nature Research Reporting Summary linked to this article.

Data availability

Microarray transcriptomic data generated in the current study have been submitted to the ArrayExpress repository, accession E-MTAB-10192. All other source data are included in the article as supplementary raw data.

Received: 28 August 2020; Accepted: 12 May 2021;

Published online: 11 June 2021

References

- Somerville, C. et al. Toward a systems approach to understanding plant cell walls. *Science* **306**, 2206–2211 (2004).
- Kubicek, C. P., Starr, T. L. & Glass, N. L. Plant cell wall-degrading enzymes and their secretion in plant-pathogenic fungi. *Annu. Rev. Phytopathol.* **52**, 427–451 (2014).
- Vaahtera, L., Schulz, J. & Hamann, T. Cell wall integrity maintenance during plant development and interaction with the environment. *Nat. Plants* **5**, 924–932 (2019).
- Engelsdorf, T. et al. The plant cell wall integrity maintenance and immune signaling systems cooperate to control stress responses in *Arabidopsis thaliana*. *Sci. Signal.* **11**, ea03070 (2018).
- Bacete, L., Mérida, H., Miedes, E. & Molina, A. Plant cell wall-mediated immunity: cell wall changes trigger disease resistance responses. *Plant J.* **93**, 614–636 (2018).
- Vaahe-Kolstad, G. et al. An oxidative enzyme boosting the enzymatic conversion of recalcitrant polysaccharides. *Science* **330**, 219–222 (2010).
- Blanco-Ulate, B. et al. Genome-wide transcriptional profiling of *Botrytis cinerea* genes targeting plant cell walls during infections of different hosts. *Front. Plant Sci.* **5**, 1–16 (2014).
- Eijsink, V. G. H. et al. On the functional characterization of lytic polysaccharide monoxygenases (LPMOs). *Biotechnol. Biofuels* **12**, 58 (2019).
- Bissaro, B., Kommedal, E., Röhr, Å. K. & Eijsink, V. G. H. Controlled depolymerization of cellulose by light-driven lytic polysaccharide oxygenases. *Nat. Commun.* **11**, 890 (2020).
- Westereng, B. et al. Efficient separation of oxidized cello-oligosaccharides generated by cellulose degrading lytic polysaccharide monoxygenases. *J. Chromatogr. A* **1271**, 144–152 (2013).
- Muraleedharan, M. N. et al. Effect of lignin fractions isolated from different biomass sources on cellulose oxidation by fungal lytic polysaccharide monoxygenases. *Biotechnol. Biofuels* **11**, 296 (2018).
- Frommhagen, M. et al. Boosting LPMO-driven lignocellulose degradation by polyphenol oxidase-activated lignin building blocks. *Biotechnol. Biofuels* **10**, 121 (2017).
- Cannella, D. et al. Light-driven oxidation of polysaccharides by photosynthetic pigments and a metalloenzyme. *Nat. Commun.* **7**, 11134 (2016).
- Tan, T.-C. et al. Structural basis for cellobiose dehydrogenase action during oxidative cellulose degradation. *Nat. Commun.* **6**, 7542 (2015).
- Kracher, D. et al. Extracellular electron transfer systems fuel cellulose oxidative degradation. *Science* **352**, 1098–1101 (2016).
- Cragg, S. M. et al. Lignocellulose degradation mechanisms across the Tree of Life. *Curr. Opin. Chem. Biol.* **29**, 108–119 (2015).
- Busk, P. K. & Lange, L. Classification of fungal and bacterial lytic polysaccharide monoxygenases. *BMC Genomics* **16**, 368 (2015).
- Jagadeeswaran, G., Veale, L. & Mort, A. J. Do lytic polysaccharide monoxygenases aid in plant pathogenesis and herbivory? *Trends Plant Sci.* **26**, 142–155 (2021).
- Jones, J. D. G. & Dangl, J. L. The plant immune system. *Nature* **444**, 323–329 (2006).
- Jones, J. D. G., Vance, R. E. & Dangl, J. L. Intracellular innate immune surveillance devices in plants and animals. *Science* **354**, aaf6395 (2016).
- Albert, I., Hua, C., Nürnberger, T., Pruitt, R. N. & Zhang, L. Surface sensor systems in plant immunity. *Plant Physiol.* **182**, 1582–1596 (2020).
- Chinchilla, D. et al. A flagellin-induced complex of the receptor FLS2 and BAK1 initiates plant defence. *Nature* **448**, 497–500 (2007).
- Couto, D. & Zipfel, C. Regulation of pattern recognition receptor signalling in plants. *Nat. Rev. Immunol.* **16**, 537–552 (2016).
- Tian, W. et al. A calmodulin-gated calcium channel links pathogen patterns to plant immunity. *Nature* **572**, 131–135 (2019).
- Bigeard, J., Colcombet, J. & Hirt, H. Signaling mechanisms in pattern-triggered immunity (PTI). *Mol. Plant* **8**, 521–539 (2015).
- Lee, D. H. et al. Regulation of reactive oxygen species during plant immunity through phosphorylation and ubiquitination of RBOHD. *Nat. Commun.* **11**, 1–16 (2020).
- Yu, X., Feng, B., He, P. & Shan, L. From chaos to harmony: responses and signaling upon microbial pattern recognition. *Annu. Rev. Phytopathol.* **55**, 109–137 (2017).
- Dodds, P. N. & Rathjen, J. P. Plant immunity: towards an integrated view of plant–pathogen interactions. *Nat. Rev. Genet.* **11**, 539–548 (2010).
- Ahuja, I., Kissen, R. & Bones, A. M. Phytoalexins in defense against pathogens. *Trends Plant Sci.* **17**, 73–90 (2012).
- Brutus, A., Sicilia, F., Maccone, A., Cervone, F. & De Lorenzo, G. A domain swap approach reveals a role of the plant wall-associated kinase 1 (WAK1) as a receptor of oligogalacturonides. *Proc. Natl Acad. Sci. USA* **107**, 9452–9457 (2010).
- Voxeur, A. et al. Oligogalacturonide production upon *Arabidopsis thaliana*–*Botrytis cinerea* interaction. *Proc. Natl Acad. Sci. USA* **116**, 19743–19752 (2019).
- Claverie, J. et al. The cell wall-derived xyloglucan is a new DAMP triggering plant immunity in *Vitis vinifera* and *Arabidopsis thaliana*. *Front. Plant Sci.* **9**, 1725 (2018).
- de Azevedo Souza, C. et al. Cellulose-derived oligomers act as damage-associated molecular patterns and trigger defense-like responses. *Plant Physiol.* **173**, 2383–2398 (2017).
- Johnson, J. M. et al. A poly(A) ribonuclease controls the cellotriase-based interaction between *Piriformospora indica* and its host *Arabidopsis*. *Plant Physiol.* **176**, 2496–2514 (2018).
- Oelmüller, R. Sensing environmental and developmental signals via cellobioses. *J. Plant Physiol.* **229**, 1–6 (2018).
- Kadowaki, M. A. S. et al. A fast and easy strategy for lytic polysaccharide monoxygenase-cleavable His6-Tag cloning, expression, and purification. *Enzyme Microb. Technol.* **143**, 109704 (2021).
- Gravino, M., Savatin, D. V., MacOne, A. & De Lorenzo, G. Ethylene production in *Botrytis cinerea*- and oligogalacturonide-induced immunity requires calcium-dependent protein kinases. *Plant J.* **84**, 1073–1086 (2015).
- Birkenbihl, R. P., Kracher, B., Roccaro, M. & Somssich, I. E. Induced genome-wide binding of three *Arabidopsis* WRKY transcription factors during early MAMP-triggered immunity. *Plant Cell* **29**, 20–38 (2017).
- Zarattini, M. et al. The bile acid deoxycholate elicits defences in *Arabidopsis* and reduces bacterial infection. *Mol. Plant Pathol.* **18**, 540–554 (2017).
- Pignocchi, C. & Foyer, C. H. Apoplastic ascorbate metabolism and its role in the regulation of cell signalling. *Curr. Opin. Plant Biol.* **6**, 379–389 (2003).
- Denoux, C. et al. Activation of defense response pathways by OGs and Flg22 elicitors in *Arabidopsis* seedlings. *Mol. Plant* **1**, 423–445 (2008).
- Frerigmann, H. et al. Regulation of pathogen-triggered tryptophan metabolism in *Arabidopsis thaliana* by MYB transcription factors and indole glucosinolate conversion products. *Mol. Plant* **9**, 682–695 (2016).
- Chen, L. Q. et al. Sugar transporters for intercellular exchange and nutrition of pathogens. *Nature* **468**, 527–532 (2010).

44. Chong, J. et al. The SWEET family of sugar transporters in grapevine: VvSWEET4 is involved in the interaction with *Botrytis cinerea*. *J. Exp. Bot.* **65**, 6589–6601 (2014).
45. Barco, B., Kim, Y. & Clay, N. K. Expansion of a core regulon by transposable elements promotes Arabidopsis chemical diversity and pathogen defense. *Nat. Commun.* **10**, 3444 (2019).
46. Ferrari, S. et al. Resistance to *Botrytis cinerea* induced in arabidopsis by elicitors is independent of salicylic acid, ethylene, or jasmonate signaling but requires PHYTOALEXIN DEFICIENT3. *Plant Physiol.* **144**, 367–379 (2007).
47. He, Y. et al. The arabidopsis pleiotropic drug resistance transporters PEN3 and PDR12 mediate camalexin secretion for resistance to *Botrytis cinerea*. *Plant Cell* **31**, 2206–2222 (2019).
48. Davidsson, P. et al. Short oligogalacturonides induce pathogen resistance-associated gene expression in *Arabidopsis thaliana*. *BMC Plant Biol.* **17**, 19 (2017).
49. Eibinger, M. et al. Cellulose surface degradation by a lytic polysaccharide monooxygenase and its effect on cellulase hydrolytic efficiency. *J. Biol. Chem.* **289**, 35929–35938 (2014).
50. Yuan, N. et al. STRESS INDUCED FACTOR 2, a leucine-rich repeat kinase regulates basal plant pathogen defense. *Plant Physiol.* **176**, 3062–3080 (2018).
51. Chan, C. et al. STRESS INDUCED FACTOR 2 regulates arabidopsis stomatal immunity through phosphorylation of the anion channel SLAC1. *Plant Cell* **32**, 2216–2236 (2020).
52. Zarattini, M. et al. Every cloud has a silver lining: how abiotic stresses affect gene expression in plant pathogen-interactions. *J. Exp. Bot.* **72**, 1020–1033 (2021).
53. Locci, F. et al. An *Arabidopsis berberine* bridge enzyme-like protein specifically oxidizes cellulose oligomers and plays a role in immunity. *Plant J.* **98**, 540–554 (2019).
54. Hahn, M. G., Darvill, A. G. & Albersheim, P. Host-pathogen interactions. *Plant Physiol.* **68**, 1161–1169 (1981).
55. Voxeur, A. & Höfte, H. Cell wall integrity signaling in plants: ‘to grow or not to grow that’s the question’. *Glycobiology* **26**, 950–960 (2016).
56. Hao, M. et al. Recombinant protein production facility for fungal biomass-degrading enzymes using the yeast *Pichia pastoris*. *Front. Microbiol.* **6**, 1002 (2015).
57. Edgar, R. C. MUSCLE: a multiple sequence alignment method with reduced time and space complexity. *BMC Bioinformatics* **5**, 113 (2004).
58. Kumar, S., Stecher, G., Li, M., Nnyaz, C. & Tamura, K. MEGA X: molecular evolutionary genetics analysis across computing platforms. *Mol. Biol. Evol.* **35**, 1547–1549 (2018).
59. Larionov, A., Krause, A. & Miller, W. R. A standard curve based method for relative real time PCR data processing. *BMC Bioinformatics* **6**, 62 (2005).
60. Reimand, J. et al. Pathway enrichment analysis and visualization of omics data using g:Profiler, GSEA, Cytoscape and EnrichmentMap. *Nat. Protoc.* **14**, 482–517 (2019).
61. Castrillo, G. et al. Root microbiota drive direct integration of phosphate stress and immunity. *Nature* **543**, 513–518 (2017).
62. Shannon, P. et al. Cytoscape: a software environment for integrated models of biomolecular interaction networks. *Genome Res.* **13**, 2498–2504 (2003).
63. Zarattini, M., De Bastiani, M., Bernacchia, G., Ferro, S. & De Battisti, A. The use of ECAS in plant protection: a green and efficient antimicrobial approach that primes selected defense genes. *Ecotoxicology* **24**, 1996–2008 (2015).
64. Chung, H. S. & Sheen, J. MAPK assays in Arabidopsis MAMP-PRR signal transduction. *Methods Mol. Biol.* **1578**, 155–166 (2017).
65. Xiao, Q. et al. Natural genetic variation of *Arabidopsis thaliana* root morphological response to magnesium supply. *Crop Pasture Sci.* **66**, 1249–1258 (2015).

Acknowledgements

This work was supported by FNRS-MIS LUX-project F.4502.19 starting grant to D.C. (M.Z. and A.M.) and PINT-BILAT-M R.M012.18; also by INNOVIRIS – 2019-Bridge-4: Re4Bru (M.A.K., S.M.) for productions of LPMOs and FER-2017 for the HPAEC-

PAD analytical platform. We thank Professor Cédric Delporte of the Analytical Platform of the Faculty of Pharmacy (APFP), ULB for the mass spectrometry of camalexin. APFP is supported by Belgian National Fund for Scientific Research (FRS-FNRS) and ULB funds (FRS No. 3.4553.08 and T.0136.13; ULB FER-2007; FER-2013; FER-2019 and Platform funds). We also thank Dr. Laurent Grumiau and Dr. Florence Rodriguez (ULB, molecular biology platform) for technical assistance during immunoblotting analysis. M.C. is a Research Associate of the INRAE (France). The IJPB benefits from the support of Saclay Plant Sciences-SPS (ANR-17-EUR-0007). This work has benefited from the support of IJPB’s Plant Observatory technological platforms and Dr. G. Mouille for SA and JA mass spectrometric analysis. We are grateful to Dr. Marie-Christine Soulié for providing *B. cinerea* B05.10 strain and Dr. Herman Höfte for providing us *BAK1* and *THE1* loss-of-function lines, all from IJPB-INRAE-Versailles, FR. Finally, the authors are deeply grateful to the reviewers for providing exceptional meaningful revision suggesting experiments that markedly improved the final output of the work.

Author contributions

M.Z. and D.C. conceptualized, planned and executed experiments and plant growth and treatments. M.Z. performed transcriptome, plant physiology, phytopathology, immunoblotting tests, and analytics. M.Z., A.M., and I.M. performed the qRT-PCR analyses. M.A.K., S.M., M.O.d.G., A.M., and D.C. cloned the enzymes and performed HPAEC and LPMO biochemistry. M.Z. and M.C. performed bioinformatics, GO, and network analysis. M.Z., S.J., and M.F. performed metabolite extractions and callose staining. M.Z. and I.M. performed western blot analysis. M.Z. and D.C. wrote the paper with contributions from all the co-authors. D.C. conceptualized and supervised the work, obtained grants, set analytical equipment, established plant growth conditions, and enzymatic cloning platform. All authors read and approved the manuscript for publication.

Competing interests

The authors declare no competing interests.

Additional information

Supplementary information The online version contains supplementary material available at <https://doi.org/10.1038/s42003-021-02226-7>.

Correspondence and requests for materials should be addressed to D.C.

Peer review information *Communications Biology* thanks the anonymous reviewers for their contribution to the peer review of this work.

Reprints and permission information is available at <http://www.nature.com/reprints>

Publisher’s note Springer Nature remains neutral with regard to jurisdictional claims in published maps and institutional affiliations.



Open Access This article is licensed under a Creative Commons Attribution 4.0 International License, which permits use, sharing, adaptation, distribution and reproduction in any medium or format, as long as you give appropriate credit to the original author(s) and the source, provide a link to the Creative Commons license, and indicate if changes were made. The images or other third party material in this article are included in the article’s Creative Commons license, unless indicated otherwise in a credit line to the material. If material is not included in the article’s Creative Commons license and your intended use is not permitted by statutory regulation or exceeds the permitted use, you will need to obtain permission directly from the copyright holder. To view a copy of this license, visit <http://creativecommons.org/licenses/by/4.0/>.

© The Author(s) 2021